A two-stage numerical analysis approach for the assessment of the settlement response of the pre-damaged historic Hoca Pasha Mosque

Dalgic, Korhan Deniz; Hendriks, Max A.N.; Ilki, Alper; Broere, Wout

DOI
10.1080/15583058.2018.1469174

Publication date
2018

Document Version
Final published version

Published in
International Journal of Architectural Heritage

International Journal of Architectural Heritage
Conservation, Analysis, and Restoration

ISSN: 1558-3058 (Print) 1558-3066 (Online) Journal homepage: https://www.tandfonline.com/loi/uarc20

A two-stage numerical analysis approach for the assessment of the settlement response of the pre-damaged historic Hoca Pasha Mosque

Korhan Deniz Dalgic, Max A.N. Hendriks, Alper Ilki & Wout Broere

To cite this article: Korhan Deniz Dalgic, Max A.N. Hendriks, Alper Ilki & Wout Broere (2019) A two-stage numerical analysis approach for the assessment of the settlement response of the pre-damaged historic Hoca Pasha Mosque, International Journal of Architectural Heritage, 13:5, 704-724, DOI: 10.1080/15583058.2018.1469174

To link to this article: https://doi.org/10.1080/15583058.2018.1469174

INTERNATIONAL JOURNAL OF ARCHITECTURAL HERITAGE
2019, VOL. 13, NO. 5, 704–724
https://doi.org/10.1080/15583058.2018.1469174

Taylor & Francis
Taylor & Francis Group

A two-stage numerical analysis approach for the assessment of the settlement response of the pre-damaged historic Hoca Pasha Mosque

Korhan Deniz Dalgic[a,b], Max A.N. Hendriks[b,c], Alper Ilki[a], and Wout Broere[d]

[a]Civil Engineering, Faculty of Civil Engineering, Istanbul Technical University, Istanbul, Turkey; [b]Structural Engineering, Faculty of Civil Engineering and Geosciences, Delft University of Technology, Delft, The Netherlands; [c]Structural Engineering, Norwegian University of Science and Technology, Trondheim, Norway; [d]GeoEngineering, Faculty of Civil Engineering and Geosciences, Delft University of Technology, Delft, The Netherlands

ABSTRACT

The current article presents a case study of the settlement response of the historic Hoca Pasha Mosque that involves uncertainties arising from the complex excavation activities, soil properties, building materials, and geometry and the presence of pre-existing cracks in the mosque's walls. The objective is to demonstrate the added value of a two-stage numerical analysis approach for the assessment of the settlement response of the building. The first stage comprises analyses of the structural behavior using the monitored settlements for each wall. The second stage examines the behavior of the complete building as a whole. The effects of soil-structure interaction and the pre-existing cracks are considered through discrete interface elements. It is shown that executed simulations can reasonably reproduce the overall settlement response, resulting stresses and the pre-existing crack activities. The parametric analyses in the second stage also produce generalizable results, of use beyond the specific case. Namely, as the soil/structure stiffness ratio increases the settlement-induced vulnerability increases. Including soil-structure interaction in the analyses reduces tensile strains due to differential settlements. Including pre-existing cracks reduces tensile strains in the vicinity of the cracks but results in an increase of stresses in neighboring sections.

ARTICLE HISTORY
Received 20 October 2017
Revised 28 March 2018
Accepted 16 April 2018

KEYWORDS
Damage; historic structure; interface; masonry; monitoring; settlement; soil; tunneling

1. Introduction

Large excavation works such as for tunnels, underground stations, and access shafts can result in significant amount of ground movements. The main reasons are deformations of the excavation support structure, alternation in the stress state in the soil depending on the soil removal, and changes in groundwater pressure and drainage conditions (Boscardin 1980). Additionally, the excavation size, construction technique, and the details of supporting system are influential on the magnitude of the resultant ground movements (Son 2003). Differential vertical settlements resulted from one or more of these sources are more critical than the uniform settlements and can damage nearby buildings by acting on their foundations. In response, the buildings resist with their overall stiffness. Eventually, the building response becomes a function of the interaction between soil and building.

Well-documented case studies in which different types of excavation, soil, and building conditions are examined offer a great resource to understand this complicated interaction problem. A number of case studies representing various circumstances from different countries have been published (Burland et al. 2001; Amorosi et al. 2014; Bryson and Kotheimer 2011; Finno, Bryson, and Calvello 2002; Fu et al. 2014; Korff et al. 2012; Pujades et al. 2015). In many studies (Burd et al. 2000; Fargnoli et al. 2015; Giardina, Hendriks, and Rots 2015; Losacco, Burghignoli, and Callisto 2014; Pickhaver, Burd, and Houlsby 2010), finite element simulations are used with different levels of sophistication of the geometrical and material modeling. In some numerical studies (Giardina, Hendriks, and Rots 2015; Son and Cording 2011), the effect of initial building damage is also considered. However, due to lack of detailed information and other uncertainties regarding excavations, foundations, soil properties, and structures, a series of assumptions and simplifications are required to simulate the actual case, which are difficult to be verified.

The current article also presents a typical case study in which several uncertainties are shown along with the considered assumptions and simplifications. Table 1

CONTACT Korhan Deniz Dalgic dalgickorhandeniz@gmail.com Civil Engineering, Faculty of Civil Engineering, Istanbul Technical University, Istanbul, Turkey.

Color versions of one or more of the figures in the article can be found online at www.tandfonline.com/uarc.

Table 1. Characterizing the Hoca Pasha Mosque case study in terms of its geotechnical and structural complexity and the availability of (monitoring) data.

Aspect	Complexity level	Data availability level
Excavations activities	High	Detailed (through the continuous monitoring data and reports regarding tunnel and shaft construction and supporting)
Soil structure	Moderate	Standard (through the reports derived from the basic in-situ soil tests)
Building deformation (building settlement and crack progress)	Moderate	Detailed (through the continuous settlement and crack monitoring data)
Building structure (geometry and material properties)	Low	Standard (through the in-situ drawings, previous expertise and publications on similar historic structures in the region)
Existing damages (crack locations and initial crack severity)	Moderate	Detailed (through the conditional building survey)

characterizes the present case with regard to excavation and construction works, soil, building deformation, building structure and pre-existing damages. It indicates the complexity and the availability of (monitoring) data for each aspect. Typical for this case study is that the initial damage is relatively well known; the building has clearly localized cracks, which have been monitored during the excavation works. By contrast, the excavation history is relatively complicated.

The originality is to simulate and assess the settlement response of the pre-damaged historic Hoca Pasha Mosque using a two-stage numerical analysis approach. According to this, first the structural model with and without pre-existing cracks is verified in a way that each façade wall is loaded separately using the measured settlements and taking into account flange affects (stiffness contribution) of other connecting walls. This stage to a large extend reduces modeling uncertainties. In the second stage, the effects of other parameters, i.e., the building stiffness, bedding stiffness, and combined settlement field due to sequential excavation works are investigated. This naturally increases the modeling uncertainties, but it more closely resembles the practice of *predicting* settlement responses. Although the mentioned stages are not dependent directly on each other, the staging approach helps to verify the building model. Besides an examination of the specific case, more generic results are obtained through parametric analyses performed in the second stage.

2. Description of the mosque and the neighboring excavation works

A comprehensive railway transportation project, namely Marmaray, was implemented in Turkey between 2006 and 2013. As part of this project, intensive tunnel and shaft excavations were carried out in the most historic parts of Istanbul.

In the Hoca Pasha district, 135 buildings were inspected in total. Fifty-eight out of 135 buildings were considered to be of moderate or high risk. These buildings were re-investigated more precisely in the detailed assessment stage. Furthermore, during the subsequent stages of the tunnel and shaft construction, evaluations were revised for some of these buildings according to increasing displacements, developing damages, and the state of excavation. The Hoca Pasha Mosque as a listed historic structure was one of these buildings affected by the shaft and tunnel excavations of the Sirkeci Station in the Hoca Pasha district.

The Hoca Pasha Mosque was rebuilt in 1868 replacing the previous one destroyed by a fire (Sefer and Ahunbay 2015). As seen in as-is drawings shown in Figure 1a, the main structural system of the mosque relies on plastered 900 mm thick load bearing masonry walls made of solid bricks and mortar joints. An outbuilding with a separate reinforced concrete frame system was built next to the main building (Figure 1a). The mosque has large arched windows (w × h: 1840 × 3860 mm) in all of the façades and doors in the northwest (NW) and northeast (NE) façades (Figure 1b–d). An internal wall of almost half of the storey height divides the narthex and prayer hall. The mosque is actually a one-story building, but there is a mezzanine floor inside. The mezzanine floor, that is constructed with steel and timber joists, and the roof are both supported by slender steel columns, situated inside the mosque, and the external masonry walls. The overall wall height is 8.25 m from the wall bottom to the eave. During the examinations, any particular foundation system was not observed except for the main walls extending approximately 1 m downward into the ground as common as in the masonry buildings constructed in the same era. On the other hand, it is assumed that the single footings are present under the internal steel columns.

The location of the mosque was considered as critical due to closeness of intensive excavation works carried out during the construction of the Sirkeci underground station. The location of the mosque and nearby excavations with

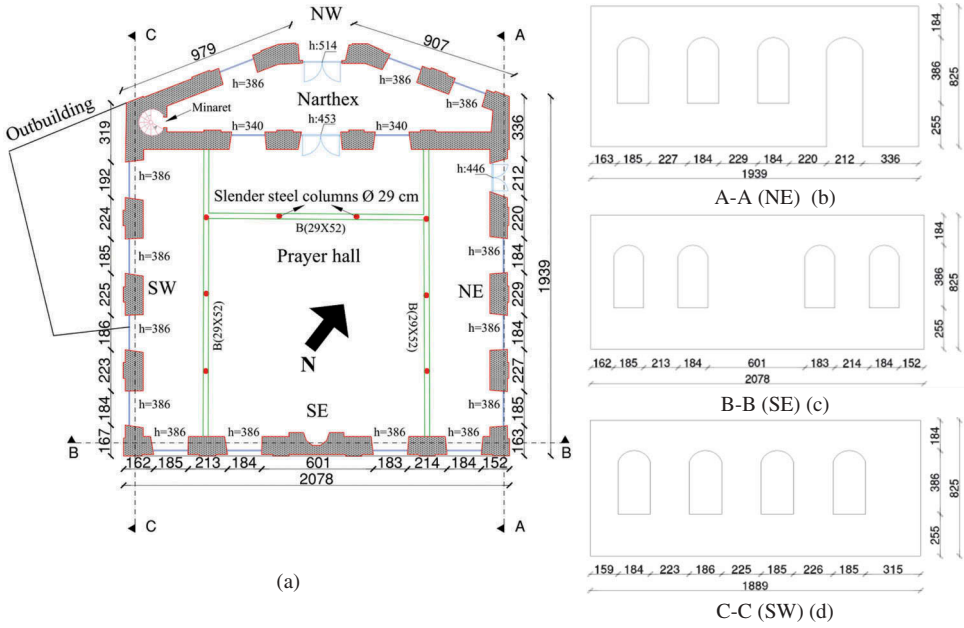

Figure 1. (a) As-is drawing of the ground floor elevation of the Hoca Pasha mosque and (b,c,d) section views (dimensions in cm) (modified from Akgun 2016).

excavation advancement directions are illustrated in Figure 2a. Monitoring results revealed that the mosque was affected to a varying extent by the indicated elliptic ventilation shaft (WVS), the pilot tunnel (NPLT) in the north platform tunnel (NPF), and the north and south ventilation chambers (NPFV and SPFV, respectively). It was observed that other excavations, namely the south platform tunnel excavation (SPF), the enlargements in north & south platform tunnels (NPF and SPF, respectively), the center walkway tunnel excavation (CE), the short connection excavations (CNVs) between NPF and SPF, and the upwardly inclined south entrance tunnel excavation (ISL) had no or less impact on the settlement response (Monthly Monitoring Reports 2008–2013) (Figures 2a and 3).

The WVS excavation wall approximates the southeast (SE) façade at 10 m. The shaft diameter is 26.4 m on the long axis and 22.8 m on the short axis. The entire shaft depth is 58 m. The first 21 m of the shaft excavation (the upper shaft) was constructed using a secant pile wall technique. For this purpose, grouted and reinforced concrete piles with 900 mm diameter were consecutively cast on the perimeter of the elliptic shaft. Then, their tips were capped with a rigid reinforced concrete ring beam (b × h: 1000 × 1500 mm). As the excavation proceeds, piles were connected circumferentially by reinforced concrete ring beams (b × h: 1000 × 1000 mm) cast at every 1500 mm. The ring beams significantly increase the radial rigidity of the circular shaft. The remaining 37 m of the excavation (the lower shaft) was carried out in the bedrock as a stepwise open face excavation, supported by a thick wall consisting of wire-meshed shotcrete and HEB 200/100 steel profiles, fixed via rock bolts. No internal cross strutting was used at any stage of the shaft excavation, not to block the equipment access through the shaft (Method Statements for Excavation and Support Works 2008).

The excavations of the tunnels (NPF, SPF, hereinafter referred to together as PFs, and CE) and the ventilation chambers (NPFV and SPFV, hereinafter referred to together as PFVs) were carried out using the New Austrian Tunnelling Method (NATM), approximately 50 m beneath the ground surface. The PFVs have the largest cross-section with 17 m diameter among all tunnels excavated for the Sirkeci Station. The length of the PFVs is 35 m. While the NPFV partly under-passes the mosque at a skewed angle, the center line of the SPFV is at a 40 m in plan distance from the closest corner of the mosque (Figures 2a and 3). In order to increase the face stability and limit deformations, tunnel cross-sections larger than 50 m^2 (as the PFs and PFVs) were divided into sub-sections (Figure 2b). Then, each sub-section was excavated sequentially starting from the pilot tunnel sub-section (respectively succeeded by the excavation of the top heading, the medium heading, the bench cut, and the invert). The NPLT, which became quite influential on the mosque settlements, was actually a sub-section excavation of the NPF having a 27 m^2 cross-sectional area (Method Statements for Excavation and Support Works 2008).

Table 2 presents starting and completion dates of the neighboring excavations. Observations regarding the influence of these excavations on the mosque behavior are listed in the last column. Before the tunnel and ventilation

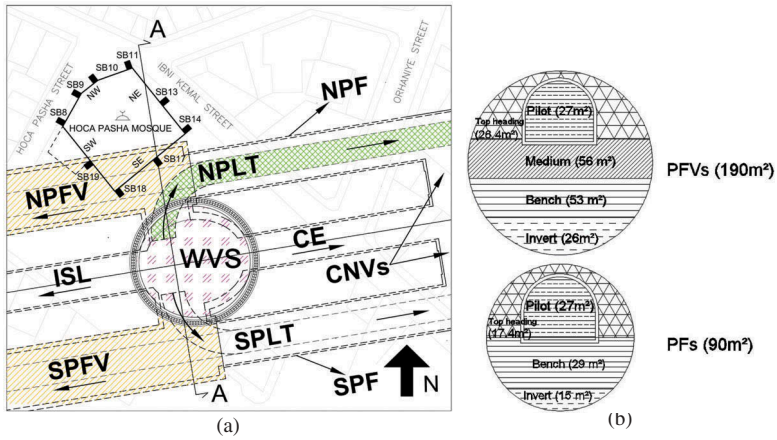

Figure 2. (a) Location and neighboring excavation works and (b) tunnel cross-sections (modified from Method Statements for Excavation and Support Works 2008).

Table 2. Starting and completion dates of neighboring excavations.

Excavation name (by sequence)		Starting date	Completion date	Observed influence on the mosque
WVS	Secant piled wall installation + Upper shaft excv. (21 m) + archaeological surveys	February 2006	February 2008	Negligible impact. Settlements up to max. 1.5 mm at the southeast façade
	Lower shaft excavation (37 m)	February 2008	July 2008	Influential from start to the end
SPF (SPLT and other sub-section enlargements)		November 2008	June 2010	No influence, neither from pilot nor from enlargement excavations
NPF (NPLT and other sub-section enlargements)		December 2008	August 2010	Substantial influence, especially from the curvilinear part of the pilot excavation
SPFV	Pilot	January 2010	February 2010	The pilot tunnel excavation was not influential
	Sub-section enlargements	March 2010	July 2010	The enlargements were influential
NPFV	NPFV pilot	April 2010	July 2010	Substantial influence for all excavation stages
	Top heading	August 2010	October 2010	
	Medium	October 2010	December 2010	
	Bench & Invert	December 2010	January 2011	

chamber excavations started, the WVS excavation had been completed on July 31, 2008. After taking down the excavation machines through the WVS, the pilot tunneling works in the PFs (SPLT and NPLT, respectively) started from the inside of the WVS. After following a curvilinear route, they proceeded eastward, moving away from the WVS and accordingly from the mosque (Figure 2a). The sequentially enlargement excavations were then started for SPLT and NPLT excluding the curvilinear sections near to the mosque. Afterward, the pilot tunnel excavation backward into the SPFV commenced and it was followed by the enlargement excavations in this section. Finally, the pilot tunnel and enlargement excavations in the NPFV were completely carried out. The difference in timing of the excavation of the WVS, NPLT, and NPFV excavations particularly offers an opportunity to investigate the accumulating effects on the mosque.

3. Local site condition

Borehole results revealed that the underlying geological structure in the vicinity of the mosque consists of three main layers (Geological Report 2008; Pressuremeter Test Results 2009). For the A-A section, indicated in Figure 2a, the obtained soil profile is shown in Figure 3. The first 15 m from the ground surface is man-made fill, consisting of sand, gravel, and clay (I). Measurements made in surrounding wells (in 2013) showed that the ground water table is also around 15 m beneath the surface. The second layer (II), which is not thicker than 10 m, is composed of clayey silty sand with shell fragments. The third layer (III) is identified as a greywacke mass, comprised of mudstone, sandstone, and claystone, which are the components of the Trakya Formation. The sections shown with IV are identified as diabase.

The mechanical properties of the main geological layers are listed in Table 3. In this table, E_s, ν, γ_s, c, and φ show the Young's modulus, Poisson's ratio, volumetric weight, cohesion, and angle of internal friction, respectively. Note that these are the values reported in the borehole test reports (Pressuremeter Test Results 2009).

4. Monitoring results and observed response

An intensive monitoring program was performed, starting from 2008 to the end of 2013. Settlements of

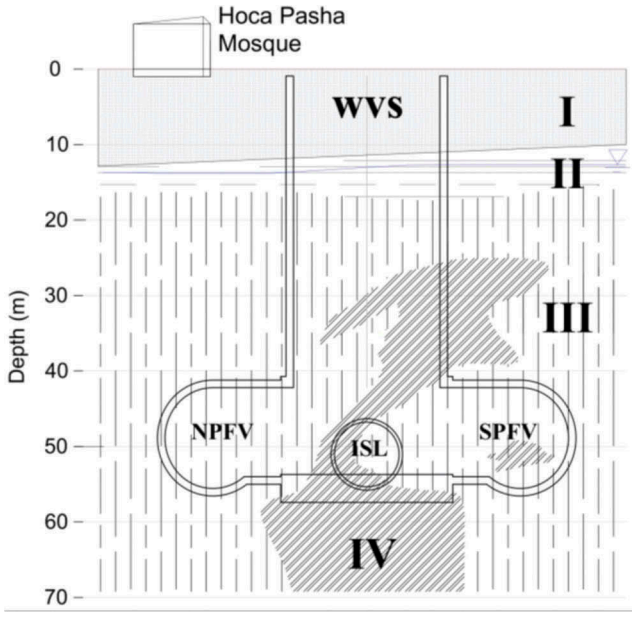

Figure 3. Sectional view of the excavation site and geological sections (A-A section in Figure 2a) (modified from Method Statements for Excavation and Support Works 2008).

the mosque were measured via leveling instruments by reading the vertical displacements of the monitoring bolts (SB monitoring points in Figure 2a) attached to the external walls. Because of the absence of an effective foundation system to inhibit or reduce the ground movements which will be transferred to the walls and by means of the placement of the monitoring bolts to the bottom of the walls, just few centimeters away from the ground surface, any significant modification in the settlement readings would not be expected. Free-field ground settlements could not be measured effectively due to building congestion and traffic in the region. Instead, estimated free-field settlements are used in the analyses to be explained in the following sections.

The settlement time history taken from SB monitoring points are shown in Figure 4. Excavation and construction activities which are influential on the settlement response of the mosque are also marked in this figure. Note that the settlements that occurred during the secant piled wall installation and the upper WVS excavation (i.e. the cut and cover excavation of the first 21 m) are not included in this figure. However, the monitoring reports (Monthly Monitoring Reports 2008–2013) show that the settlements at that stage were negligible (≤1.5 mm).

As expected, settlement readouts measured on the southeast (SE) (where SB14, 17, and 18 were attached) and southwest (SW) (where SB8 and 19 were attached) façades which were relatively closer to the WVS, NPLT, and NPFV excavations have been higher than the other readouts. After the completion of the WVS excavation, the rate of measured settlements of the mosque decreased, until the pilot tunnel excavations SPLT and NPLT started. Sudden increases in the slopes of the settlement vs. time curves point out that the NPLT excavation, specifically the curvilinear section, has become quite influential. Between February 2009 and

Table 3. Reported mechanical properties of the geological layers (Geological Report 2008; Pressuremeter Test Results 2009).

Soil Layer	Depth (m)	E_s (MPa)	ν	γ_s (kN/m^3)	c (kN/m^2)	φ (degree)
Man-made fill (I)	0–15	33.0	0.30	19.0	0.00	30.0
Clayey silty sand (II)	10–15	56.0	0.30	19.0	0.00	34.0
Greywacke (III)	15 to deeper	150	0.35	21.0	200	30.0

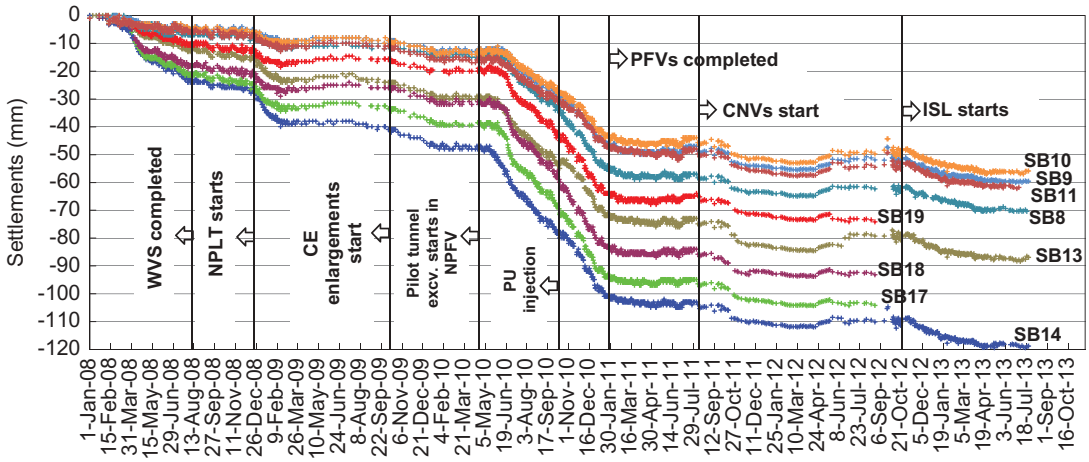

Figure 4. The settlement time-history of the mosque (modified from Monthly Monitoring Reports 2008–2013).

April 2010, an increase presumably due to CE pilot tunnel excavation and enlargement excavations in the PFs was observed. From April 2010 onward, the settlements significantly increased again. This time, the reason was the pilot tunnel and enlargement excavations in the PFVs. It should be particularly highlighted that the pilot tunnel and the enlargement excavations in the NPFV played a major role in this increase. In order to limit the settlements at that stage, two ground stabilizations and a following uplifting application were carried out. The first ground stabilization attempt was a cement injection procedure performed horizontally from the inside of the WVS towards the mosque. In addition to cement injection, horizontal steel rods were driven into the soil in order to compact the ground under the mosque. The second attempt was aiming at both ground stabilization and uplifting the severely settled parts of the mosque. For this purpose, vertical steel rods, 7 m long and 36 mm in diameter, were driven into the soil with an inclined angle at every 40 cm around the main external masonry walls. After performing a primer polyurethane (PU) injection, uplifting was performed through a secondary and deeper PU injection. Consequently, an upward movement (up to 3 mm) around SB13, 14, and 19 was obtained. The effect of uplifting can be seen in the settlement time history of SB13 in Figure 4 between September and November 2010. All of the excavation works in SPFV and NPFV tunnels were finalized towards January 2011.

4.1 Conditional survey prior to excavations

A conditional survey conducted before the commencement of the excavations revealed the presence of pre-existing localized cracks (C1, C2, C3-1, C3-2, C5, C6, and C10) in all of the façades (see Figure 5) (Detail Survey Report 2008). These cracks all began at the door and window arches, either at the vertices or closer to the bottom of the arches. They have propagated upward to the eaves almost vertically. The cracks were also visible from the inside of the mosque. While C1 and C2 above the arched door of the NE façade were the widest, C3-2 and C10 above the arched windows in the NW and SE façades were the narrowest cracks. The observed initial width of these cracks varied from 5–10 mm. The locations of the pre-existing localized cracks in the ground plan are also given in Figure 5. As is, the building was classified as moderately damaged by the inspection team considering its "prior to all excavations" and estimated post condition.

4.2 Settlement response during the construction and excavation activities

The mosque's response was regularly inspected and reported as the construction and excavation works progress (ITU Evaluation Reports 2008–2011). At the visual inspection dated January 21, 2009, slight widening of the mentioned pre-existing cracks due to the WVS and curvilinear NPLT excavation were observed. Increases in crack widths were recorded from February 12, 2009 onward. Two different methods were adopted to measure the crack openings and closures throughout the excavations. Until June 23, 2010, digital callipers were used to measure the crack widths. As of June 2010, the frequency of crack measurements was increased with regard to increasing settlements due to the NPFV excavations. A separation between the main building and the outbuilding was also observed. Considering the continuing NPFV excavations, from June 23, 2010 onward, more precise scale type crack meters were bonded and used to measure the crack widths. Although a few new cracks formed around the localized pre-existing cracks during the NPFV excavations, their widths remained relatively insignificant (none of them exceeded 0.9 mm until the end of the excavations).

Figure 6 shows the variation of the widths (crack activity) of the major pre-existing localized cracks. Although a trend cannot be given for the initial data obtained by the digital callipers for the period before June 23, 2010, the final digital calliper readouts are added to the data obtained by scale type crack meters. No measurements for crack C3-2 were carried out.

Figure 6 shows that crack C3-1 widens and closes significantly during the NPFV excavations. As the mosque settlements slow down towards March 2011, a closing is observed for this crack. Another increase in the activities of C1 and C2 is noted during the top heading and medium sub-section excavations of NPFV. The C5 and C6 cracks seem to be influenced least by the NPFV excavations. However, an increase in their widths is observed as of June 2011 possibly due to the CNV excavations. Crack C10 shows minor variation throughout the excavations.

4.3 Evaluation of the mosque's response based on the conventional deformation measures

Monitored settlement response of each external masonry wall is examined by the authors using conventional deformation measures, namely angular distortion, deflection ratio, and rigid rotation. For this purpose, the monitored wall settlement profiles are provided in Figure 7 considering seven key dates, i.e., after the completion of the WVS excavation (September 15, 2008),

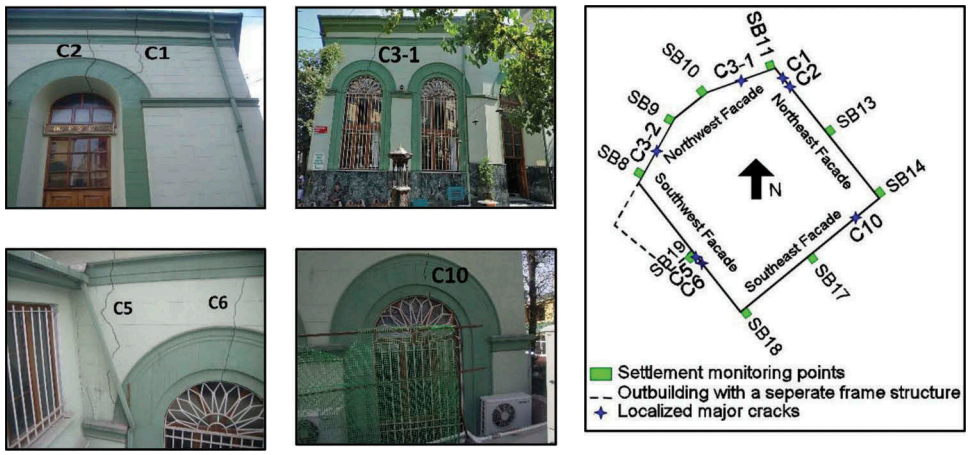

Figure 5. The pre-existing localized cracks and their locations in the plan of the mosque.

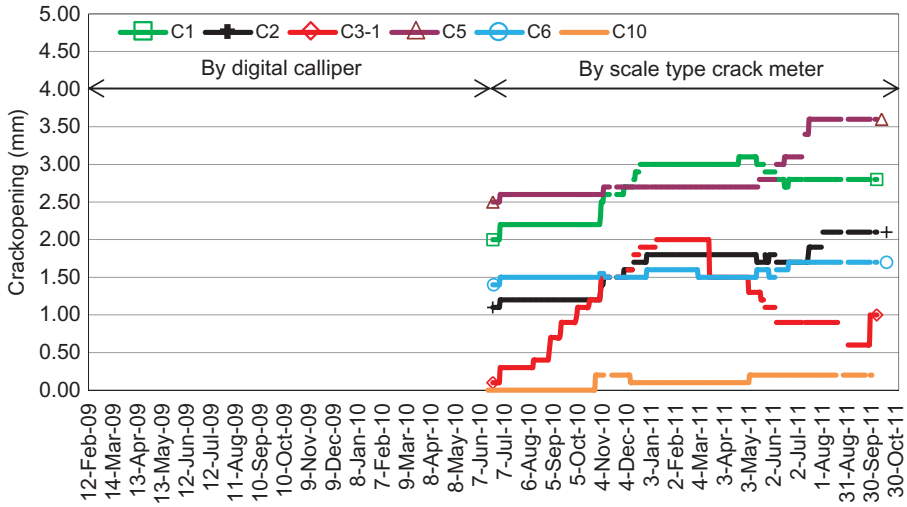

Figure 6. Opening and closures of the pre-existing localized cracks.

after the completion of the curvilinear NPLT excavation (March 24, 2009), before the NPFV excavations (March 18, 2010), after the completion of the NPFV pilot tunnel excavation (July 29, 2010), after the completion of the entire NPFV excavations (January 3, 2011) and before and after the CNV excavations (July 21, 2011 and March 1, 2012). As seen, while the SE façade experiences sagging (a convex settlement profile), the others experience hogging (a concave settlement profile) throughout the excavations.

Based on the wall settlements at these considered dates, the maximum angular distortion (β_{max}), the deflection ratio (Δ/L), and the rigid rotation (ω) values of the façade walls are calculated (Figures 8a–c, respectively). β_{max} is the largest angular distortion value (β) calculated as the rotation of the straight line connecting two adjacent monitoring points relative to their tilt (Boscardin 1980). Δ/L is the ratio of relative deflection between two monitoring points to the distance between them (Burland and Wroth 1974). ω is the rigid rotation of the façade wall defined by the settlement readouts of two outmost monitoring points. Calculation of these measures are schematically explained in Figure 8d. Three internationally accepted empirical limit values β_{max} = 0.0005 (1/2000) (Meyerhof 1982), Δ/L = 0.0003 (1/3300) (Polshin and Tokar 1957), and ω = 0.002 (1/500) (Rankin 1988) are also indicated in Figures 8a–c. The first two values show the cracking limit of unreinforced load-bearing masonry walls in hogging. Note that the Δ/L = 0.0003 value is obtained by interpolating the linear wall length to wall height ratio (L/H) vs. Δ/L relationship of Polshin and Tokar (1957). For the derivation of Δ/L = 0.0003, L/H is taken as 3. Note that the cracking limits for sagging would be higher (i.e., more tolerant). ω = 0.002 suggests the limit between negligible and slight damage.

The β_{max} vs. time and Δ/L versus time graphs in Figures 8a,b show that the wall distortions due to WVS (according to values dated September 15, 2008) and curvilinear NPLT (according to values dated on

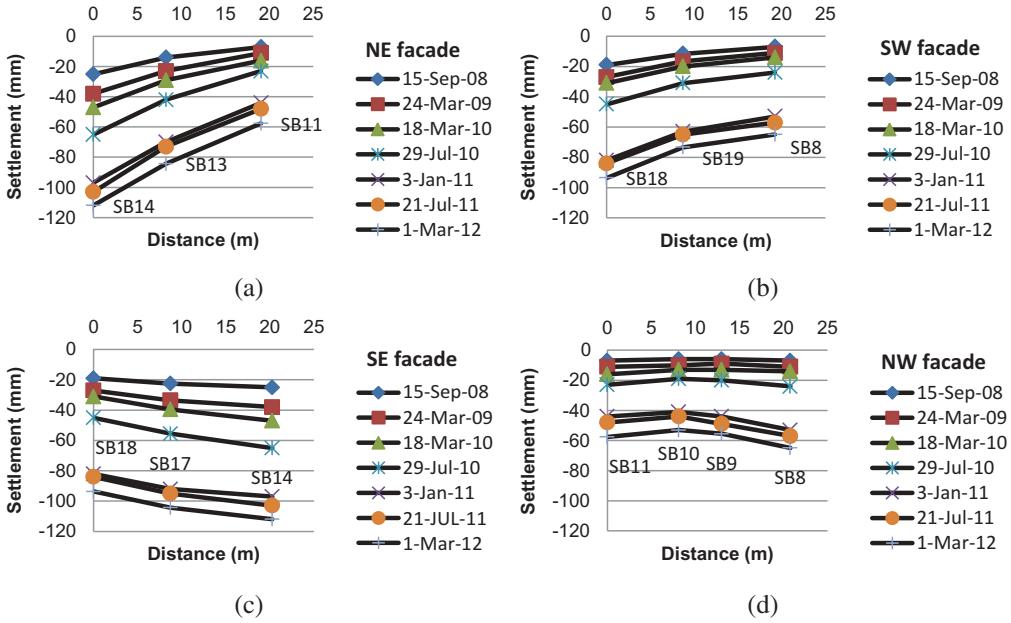

Figure 7. Monitored settlements along the main masonry walls.

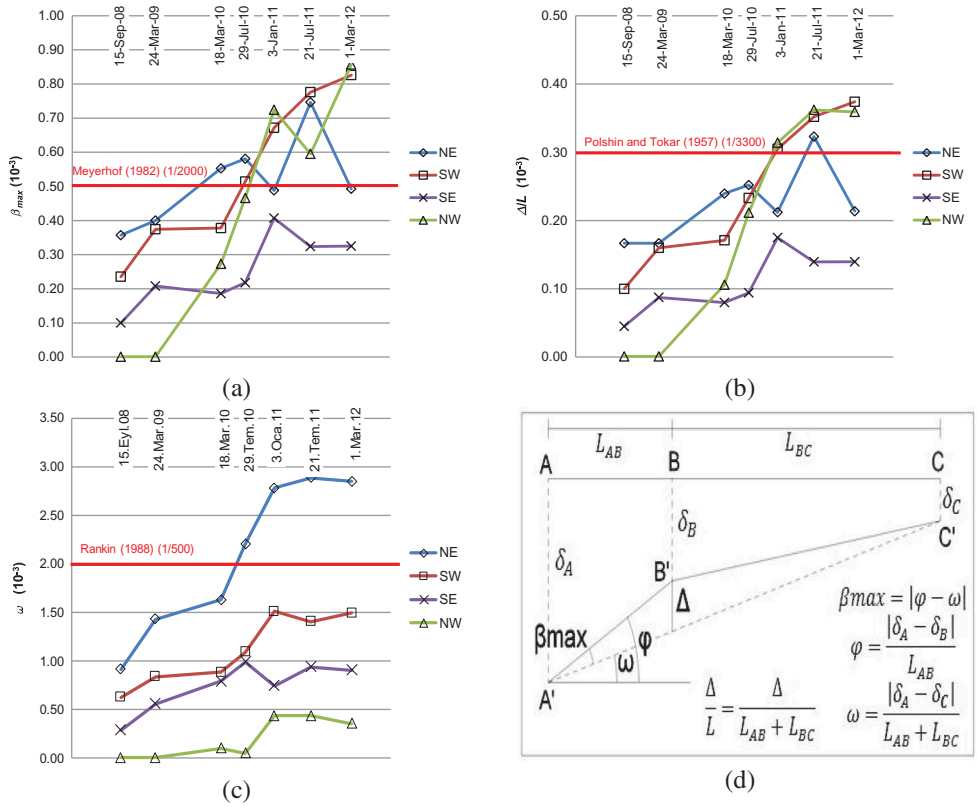

Figure 8. Calculated wall distortions: (a) angular distortion, (b) deflection ratio, and (c) rigid rotations.

March 24, 2009) excavations are lower than the proposed limit values. Enlargement excavations in CE and SPFV result in an increase in β_{max} and Δ/L values of the NE and NW walls (see the variation between March 24, 2009 and March 18, 2010). The pilot tunnel excavation in NPFV became very influential between April 2010 and July 2010. In this period, a sharp increase in the distortion values of the most of the walls is observed. Until the completion of the NPFV excavations in January 2011, the wall distortions continue increasing

with the exception of the NE wall. In the last two periods (January 3–July 21, 2011 and July 21, 2011–March 1, 2012), the NE and NW walls experience both increases and decreases in their distortions. Conversely, the distortions of the SW wall monotonically increases in these two periods. The distortions of the SE wall are relatively small. On the other hand, while the NE wall experiences the highest rigid rotation, the NW wall has the lowest value (Figure 8c). The calculated maximum rigid rotation is 0.0028 (1/345) for the NE wall and slightly exceeds the limit proposed by Rankin. From January 3, 2011 onward, rigid rotation values almost level off. At the end of the PFV excavations (January 2011), considerably different rigid rotations are experienced by the parallel NE and SW walls. Presumably, this situation might have resulted in additional shear forces in the connecting SE and NW walls and at the corner connections.

Note that the crack activities given in Figure 6 are in general agreement with the wall distortions given in Figure 8. For instance, the lowest activity in the C10 crack is in line with the lowest distortions experienced by the SE wall and the variations of the width of crack C3-1 are in line with the increases and decreases in the distortions of the NW wall. However, a direct comparison between crack activities (openings and closings) and variations of calculated wall distortions may not always be straightforward due to the following.

(1) Used crack measurement system: The crack width measurements are carried out at only one single location on the crack line, which is selected where the initial crack width is the largest. This kind of a measurement method may easily overlook the detailed crack activities (openings and closings) that can vary along the crack line.
(2) Distortion calculation method: The pre-existing cracks are local features within the entire wall and their openings and closings partly depend on local mechanisms. On the contrary, the conventional evaluation technique (Figure 8) based on the variations of two different distortion measures (angular distortion and deflection ratio) is not expected to predict such detailed and local mechanisms. Distortion measures are basically calculated to obtain a global idea regarding the settlement response of the wall. Therefore, they are mostly related to the overall response of the wall rather than a localized crack.
(3) The settlement variation between monitoring points is assumed linear. In reality, this is not perfect linear.
(4) 3D effects: There might also be out of plane bending behavior due to 3D effect of ground movements and specifications of the structural load-bearing system that will eventually cause partial crack openings or closings. (Such a numerical observation will be presented in the Section 5.)

5. Proposed two-stage numerical assessment approach

The response of the Hoca Pasha Mosque to the complicated spatial ground settlements is examined by 3D finite element modeling (DIANA v10.1 2016). For this purpose, a two-stage numerical analysis approach is used. In the first stage (in Section 5.1), the adequacy of the building model with and without pre-existing cracks is primarily verified by using monitored wall settlements. In this way, the issue of setting a realistic soil-structure interaction is temporarily put off. In the second stage, verified building model is analysed using estimated free-field ground movements considering soil-structure interaction.

The geometry of the used building model is shown in Figure 9a. Recalling that the walls have a thickness of 900 mm and diaphragm actions of the roof is not relevant for the type of loading, the mezzanine floor, the roof, the internal columns, and the minaret are not included in this model since their contribution to the overall stiffness is considered as negligible. These sections might have minor damage due to differential settlements. Since this damage will be less critical, the investigation of the response of these sections is out of focus of the current study. The masonry walls are modeled using solid tetrahedron (3 sides, 4 nodes) elements (TE12L). Meshed element size is 250 mm in all dimensions. Bricks and mortar joints are not considered separately in the model and masonry is represented homogenously using linear elastic material properties (the continuum model described previously by Lourenco 1996) (Table 4). Due to the historical character of the mosque, no destructive test on the masonry could be performed to determine the actual mechanical properties. Instead, three different Young's modulus (E_{m1}, E_{m2}, and E_{m3}) are adopted. E_{m1} and E_{m2} (350 and 1000 MPa, respectively) are assumed to cover the range of representative values of these typical load bearing masonry walls, constructed in the same era with similar techniques and materials (Ispir and Ilki 2013). The higher E_{m3} (10,000 MPa) is included to distinguish the effect of Young's modulus (Table 4).

The localized and already open pre-existing cracks are simulated with vertically aligned linear elastic discrete

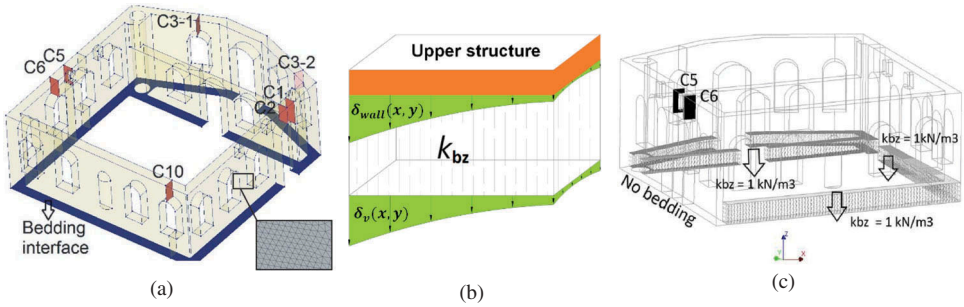

Figure 9. (a) Mosque model geometry, (b) interface model, and (c) interface configuration for the isolated SW wall.

Table 4. Assigned material parameters.

Masonry wall	Property		
	Young's modulus (MPa)	E_{m1}	350
		E_{m2}	1000
		E_{m3}	10,000
	Poisson ratio	v	0.2
	Unit weight (kg/m^3)	γ_m	1800
Localized cracks	Interface stiffness in normal direction (kN/m^3)	k_{czi}	$(E_{mi}/L_f) \times 10^6 \cong 0$
	Interface stiffness in tangential directions (kN/m^3)	$k_{cxi} = k_{cyi}$	$E_{mi} \times 10^3$
Bedding	Interface stiffness in normal direction (kN/m^3)	k_{bz1}	5000
		k_{bz2}	20,000
		k_{bz3}	40,000
		k_{bz4}	80,000

interfaces. The interface elements are triangular elements (T18IF) which are inserted between two planes in a 3D configuration. They have three opposite nodes on each side of the interface and each node has three translation degrees of freedom in x, y, and z axes. In order to reveal the effect of localized cracks, two extreme conditions are considered: cracks with very low interface stiffness (almost zero) and excluding the crack interfaces from the model (no cracks). For the former, interface stiffness values in the normal direction k_{czi} are calculated theoretically using Equation (1). That is, the interface stiffness is set as the equivalent stiffness of an fictitious masonry tie of length L_f. The very low interface (almost open) stiffness is obtained by considering L_f, arbitrarily, as 10^{10} mm. The crack interface stiffness in the tangential x and y directions (k_{cxi} and k_{cyi}, respectively) is taken as relatively small, although not extremely small, ($E_{mi} \times 10^3$ in kN/m^3) to take into account small frictional effects between crack faces and to avoid large unrealistic out-of-plane drifts of the wall portions between the cracks (Table 4):

$$k_{czi} = \frac{E_{mi}}{L_f} \times 10^6 \left(kN/m^3\right) (\sim 0 \text{ for any } Emi). \quad (1)$$

Monitored wall settlements (considered in the first stage analyses) and estimated free–field ground settlements (used in the second stage analyses) are imposed to the bedding interfaces at the bottom surfaces of the solid walls. The same element type (T18IF) as used to model the pre-existing cracks is used for the bedding. Figure 9b schematically explains the relationship between applied and resultant displacements on the each side of the bedding interfaces. In this figure, δ_v(x,y) is the applied vertical prescribed deformation and δ_{wall}(x,y) is the resultant displacement at the bottom of the walls of the structure. For the increasing values of k_{bz} the modulus of subgrade reaction (referred to as bedding stiffness hereafter) δ_{wall} approaches to δ_v, i.e., for $k_{bz} \rightarrow \infty$, $\delta_{wall} = \delta_v$. The latter is equivalent to excluding the bedding interface from the model. Lower values of k_{bz} (corresponds to a softer soil) will lead to relative displacements in the normal direction of the bedding interface, δ_v-δ_{wall}. The effect of using a nonlinear soil model in the analyses has been investigated by the previous researchers (Burd et al. 2000; Fargnoli et al. 2015). It was shown that more realistic simulations are possible by considering small-strain nonlinearity and stiffness reduction with increasing deformation in the soil model. However, in this study, a linear elastic material model with a constant bedding stiffness is used. Although the bedding stiffness is not a specific material property for soil, Bowles (1996) suggested that guide values given in Table 5 can be used to estimate the correct order of this

Table 5. Guide values proposed by Bowles (1996) for bedding stiffness.

Soil type	k_{bz} (kN/m^3)
Loose sand	4800–16,000
Medium dense sand	9600–80,000
Dense sand	64,000–128,000
Clayey medium dense sand	32,000–80,000
Silty medium dense sand	24,000–48,000
Clayey soil	12,000–24,000
$q_a \leq 200$ kPa	24,000–48,000
$200 < q_a \leq 800$ kPa	>48,000
$q_a > 800$ kPa	

Note: q_a is the allowable bearing pressure.

quantity. Utilizing Bowles's guide values, four different bedding stiffness values varying in a broad range are considered in the parametric analyses (5000, 20,000, 40,000, and 80,000 kN/m^3) (Table 4). Among these, k_{bz3} = 40,000 kN/m^3 is determined as the reference value considering the depth and type of underlying soil layers in the region. The bedding stiffness in transverse direction is assumed close to zero. Note that the bedding interface does not contribute to the flexural stiffness of the wall; its main function will be the monitoring of the relative displacement distribution underneath the walls and to simulate the effect of soil layers underneath the walls.

5.1 The first stage analysis results for building model verification by using measured settlements

In order to verify the building model, this section presents preliminary analysis results. These analysis results are based on two temporary simplifications of the numerical model.

(1) The critical issue of defining the settlement fields and a realistic bedding stiffness are avoided, by using measured wall settlements as displacement loads at the bottom of the building.
(2) The response of each load-bearing wall to the displacements imposed at the bottom of that wall is analysed for each wall separately, by ignoring the loading effects from the three remaining walls, but by including the flange effects (stiffness contribution) of other connecting walls.

As an example, Figure 9c presents the modified analysis model for the SW wall. No bedding interface is assigned at the bottom of this wall: the applied prescribed deformations (i.e., the measured settlements) will be transferred directly to the wall. The analyses performed in this section are based on the measured settlements at the end of July 2011 when NPLT, SPFV, and NPFV tunnels were completed (Figures 4 and 7b). The measured settlements are distributed along the wall length based on the assumption that the settlements are varying linearly between the monitoring points SB8, SB19, and SB18. On the other hand, an extremely soft bedding interface stiffness (1 kN/m^3) is assigned to the bottom of the remaining walls. In this way, the rest of the structure still exerts a stiffness influence on wall SW. The Young's modulus E_{m1} and E_{m3} for the masonry walls are used in successive analyses. The SW wall includes the C5 and C6 cracks (defined with a very low normal stiffness). In a variation study, these cracks are excluded. The cracks on the other walls are always excluded from the model.

Figures 10 and 11 show the deformation and crack opening results obtained for the SW wall without and with crack interfaces (C5 and C6), respectively. In the first case, it is seen that the major principal tensile strains (ε_p) concentrate around the small niche at the upper side of the wall as well as the bottom parts of the central windows. The maximum principal tensile strain (ε_{pmax}) reaches about 0.080%. This value exceeds slightly the tensile strain range (0.038–0.060%) that was previously reported by Burhouse (1969) as the onset of visible cracking in the brick masonry walls. The presence of the C5 and C6 cracks in the second case results in a remarkable change in ε_p distribution. It is seen that the C5 and C6 cracks reduce the strain levels in their vicinity, however they result in an increase in the strain levels at the bottom parts of the central windows. The maximum principal tensile strain reaches about 0.1%. In both cases, the damage class of SW wall is assessed slight damage based on the comparison made between ε_{pmax} and the suggested limiting tensile strain intervals of Boscardin and Cording (1989) (see Table A1 in the Appendix).

The variation of the relative crack displacements (δ_{cz}) along the height of the C5 and C6 cracks are shown in Figure 11b,c, respectively. Crack C6 is opening more uniformly and widely, whereas C5 widens more at the upper part and relatively less. A direct comparison of numerical and monitored crack

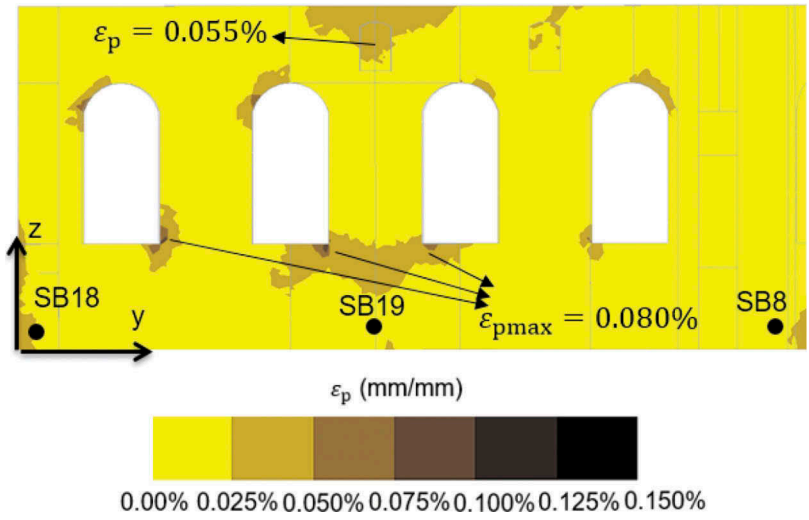

Figure 10. distribution in SW without C5 and C6 crack interfaces (E_m = 350 MPa).ε_p.

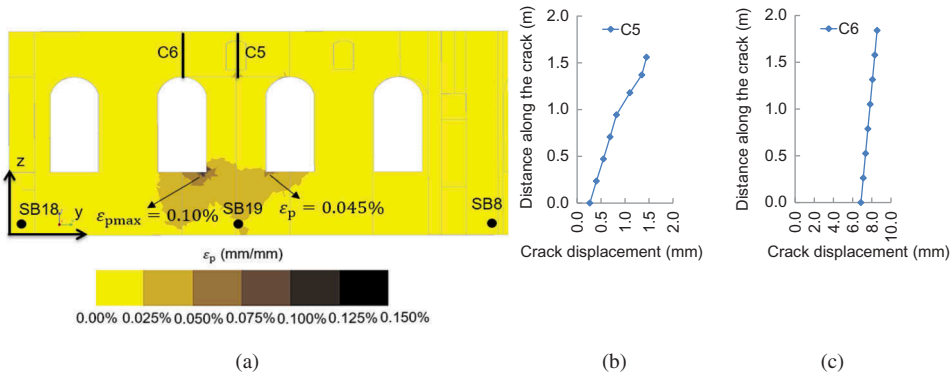

(a) (b) (c)

Figure 11. (a) ε_p distribution in SW wall with crack interfaces and relative crack displacements of (a) C5 and (b) C6 cracks (E_m = 350 MPa).

openings is not straightforward due to aforementioned restrictions. Instead, making comparisons based on the summed crack openings of the two cracks makes sense. The analysis yields that the total crack opening of C5 and C6 (C5 + C6) ranges from 7–9.5 mm from the bottom to the top of the cracks. The sum of the monitored crack openings (C5+C6) (at the end of July 2011 in Figure 6) is 5.3 mm.

Similar modeling and analysis procedures are executed for the NE, NW, and SE walls. The results obtained from these analyses are summarized in Table 6. As seen, the magnitude of shown ε_{pmax} values are relatively low as in the case of SW wall. This would result in negligible to slight damages for these walls (Table A1).

An in-plane rotation is observed for the wall portion between the C1 and C2 cracks in NE wall (Figure 12a). Due to this rotation, while the C1 closes at the upper part C2 widens and the other way around at the bottom part as observed from the outside of the mosque. For these crack interfaces, the overall relative crack displacement (δ_{cz}) from bottom to upper tip varies between −0.33 mm (closing) and 4.71 mm (opening). On the other hand, a diagonal out-of-plane rotation is observed for the C3-2 crack in the NW wall (Figure 12b). Finally, the SE wall experiences the lowest distortion compared to other walls in which the C10 crack tends to close.

Note that varying the Young's modulus of the masonry from 350 MPa (E_{m1}) to 10,000 MPa (E_{m3}) results in insignificant changes in the magnitudes of the principal strains and crack openings. As seen in Table 6, the obtained crack activities and determined damage classes based on the tensile strain levels are in line with the actual monitoring results and in-situ building observations. Recall that, during the excavation and construction works, while the pre-existing cracks were active a few new cracks of insignificant extent have occurred. The agreement between the results of the first stage analyses and reality shows the suitability of the building model and choice of the range of the elastic material parameters.

Table 6. Numerical results for NE, NW, and SE walls (with and without pre-existing cracks).

Wall	Max. principal strain (without cracks) (E_m = 350 MPa)	Max. principal strain (with cracks) (E_m = 350 MPa)	Remarks for relative crack displacements	Estimated damage class according to Table A1
NE	ε_{pmax} = 0.060% Near to upper and lower section of the central part of the wall	ε_{pmax} = 0.055% Near to upper and lower section of the central part of the wall	Figure 12a	Very slight damage in both cases
NW	ε_{pmax} = 0.075% Observed at several sections near to window and wall corners	ε_{pmax} = 0.075% Observed at several sections near to window and wall corners	Figure 12b	Slight damage in both cases
SE	ε_{pmax} = 0.025%	ε_{pmax} = 0.025%	C10 uniformly closes	Negligible damage in both cases

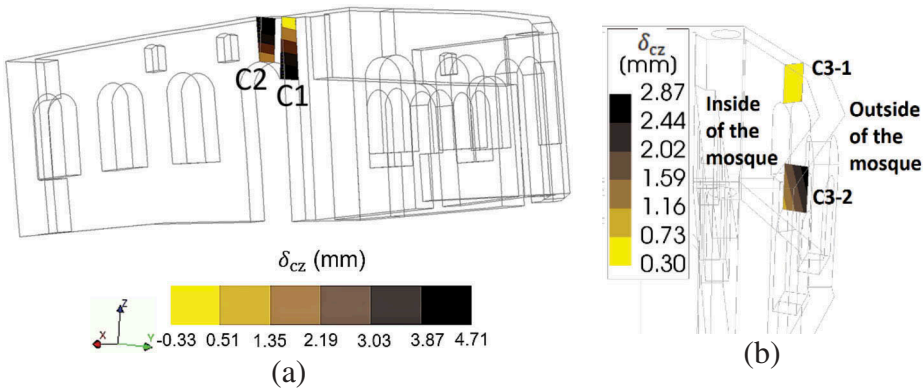

Figure 12. Rotation of crack interfaces from (a) perspective (C1&C2) and (b) side view (C3-2).

5.2 Second-stage parametric analyses performed by using estimated free-field ground settlements

In this sub-section, the settlement response of the mosque will be examined using parametric analyses based on generated settlement fields. The rational of this kind of analyses compared to the previous ones, in which measured settlements are used as input, is to offer an opportunity to examine the crack activities and overall response without having the knowledge of the building settlements. Furthermore, the effect of different masonry and bedding properties and modeling configurations (i.e., with or without crack and bedding interfaces) are investigated in this section.

Due to aforementioned limitations of in-situ free-field ground settlement data, 3D settlement fields have to be estimated. For the shaft excavation, WVS, 3D settlement field (Figure 13b) is produced based on empirical 2D free-field settlement profile curve (Figure 13a). For NPLT, SPFV, and NPFV tunnels, 3D settlement fields (Figure 13c–e) are based on reported 2D finite element models (Figure 13a). Each settlement field is formed as a vertical settlement displacement matrix and applied as a prescribed deformation load to the interfaces at the bottom of the walls. The combined settlement field (Figure 13f) is the superposition of all of the matrices formed for each separate excavation (WVS, NPLT, SPFV, and NPFV). Details of the sub-studies to estimate 3D settlement fields for WVS and tunnels are explained in the following Sections 5.2.1 and 5.2.2.

5.2.1 Derivation of the 3D settlement field for WVS from the calculated empirical ground settlements

For the estimation of free-field ground settlements and the derivation of corresponding settlement field due to the shaft excavation, the study of Moormann (2004), in which 530 case histories of retaining walls and ground movements due to deep excavations are analyzed, is used. Moorman shows that the movements of the shaft wall and the surrounding ground seem to be largely independent of the stiffness of the retaining wall system. According to the author, once a sufficient stiffness is provided, the movements are governed by other relevant factors. Thus, an additional increase of the system stiffness does not lead to a corresponding decrease of movements. Similar conclusions were obtained by Clough and O'Rourke (1990) and Long (2001). Considering this, the mixed type wall construction of the current shaft can be considered as single type wall and empirical settlement relationships proposed for uniform retaining wall constructions can be used for the entire depth of the shaft (H_e = 58 m). Moormann (2004) also shows that the maximum ground settlements (δ_{vm}) behind an excavation wall can vary in a wide range. For relatively stiff clays (undrained shear strength $c_u \geq$ 0.075 MPa), he observed that the maximum ground settlement (δ_{vm}) to excavation depth (H_e) ratio takes a value between 0% (no ground settlement) and 0.90%. The average δ_{vm}/H_e ratio is reported as 0.18%. A similar range (0.00–0.20%) for the average value of δ_{vm}/H was also previously proposed by Clough and O'Rourke (1990) and Long (2001).

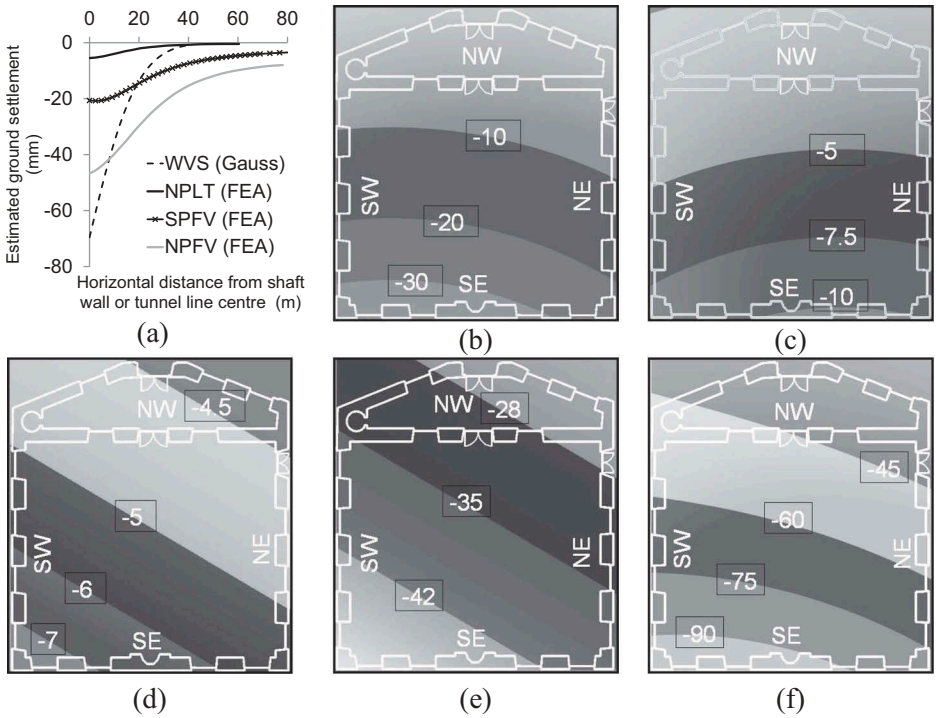

Figure 13. (a) Reported or derived 2D free-field ground settlement estimations which are used to produce settlement fields and 3D settlement field contours generated for (b) WVS, (c) NPLT, (d) SPFV, (e) NPFV, and (f) combination of WVS, NPLT, SPFV, and NPFV excavations.

In the current study, considering the magnitude of measured settlements, an average value of δ_{vm}/H_e = 0.12% which is in the proposed range can be assumed. In this case, δ_{vm} is calculated as 69.6 mm for H_e = 58 m. In order to calculate the corresponding ground settlement profile for δ_{vm}/H_e = 0.12%, Peck's (1969) Gaussian formula (Equation (2)) can be used as introduced in the study of Lee et al. (2007). This curve was originally suggested to estimate free-field ground settlement profiles due to tunneling. Afterward, Lee et al. (2007) used this function to predict the excavation-induced ground settlement profile behind an excavation wall assuming that the wall stands at the inflection point of the Gauss curve. In Equation (2), δ_v is the ground settlement at any distance r from the shaft wall and W shows the settlement trough width proposed by Caspe (1966). W can be calculated using Equation (3). Therein, H_i is settlement influence depth below the excavation level and φ is the friction angle of the soil. H_i is calculated according to Equation (4) for soils with $\varphi > 0$. φ is assumed to be 30° in the current case. B shows the excavation width and can be taken as 24.6 m as the average diameter of the elliptic shaft in the current study:

$$\delta_v = \delta_{vm}.e^{\left[0.5-0.5\left(1+\frac{2r}{W}\right)^2\right]} \quad (2)$$

$$W = (H_e + H_i)\tan(45 - \frac{\varphi}{2}) \quad (3)$$

$$H_i = 0.5B\tan(45 - \frac{\varphi}{2}) \quad (4)$$

Figure 13b shows the contours of the settlement field which is produced for the shaft excavation based on the Peck's (1969) Gaussian curve (Figure 13a). Note that the 3D settlement field was constructed by applying the 2D Gaussian curves in radial directions of the elliptical shape of the shaft starting from the position of the shaft wall.

5.2.2 Derivation of the 3D settlement fields for NPLT, SPFV, and NPFV tunnels from the 2D numerical results

Free-field ground settlements due to tunnel excavations were obtained from the numerical analysis results reported by the contractor company (Figure 13a) (Prediction of Ground Surface Settlement Report 2011). In these analyses, 2D plane strain conditions were considered. Man-made fill (I) and clayey silty sand (II) layers were modeled using an elasto-plastic Mohr-Coulomb model. Besides the elastic properties, anisotropic damage parameters were used to reduce the shear modulus of the greywacke (III). Damage parameters were determined through back analyses based on the monitored crown and spring line settlements of the concerned tunnels. Figures 13c–e show the contours of the settlement fields which are produced based on the numerical simulations

(Figure 13a). As seen, the curvilinear NPLT excavation yields curved settlement contours and the SPFV and NPFV form skewed line contours corresponding to the geometry and position of these tunnels. In line with the monitoring results of the mosque (Figure 4), the settlement contours resulting from the NPFV excavation indicate much higher settlements in comparison with the NPLT and SPFV excavations. Figure 13f shows the combination of all settlement contours resulting from the WVS shaft and NPLT, SPFV, and NPFV tunnels. Note that this combined settlement field corresponds to a site settlement stage when the NPLT, SPFV, and NPFV tunnels were completed (at the end of July 2011). A sagging due to combination of the settlement contours of the WVS and NPLT can be noted for the SE wall. The other walls are hogging. This situation is also in line with the monitored responses of these walls. However, two discrepancies between estimated and actual settlements should be highlighted and the probable reasons should be discussed.

(1) Although the estimated settlements are increasing towards the SE-SW corner (SB18) due to closeness of this corner to the WVS, SPFV, and NPFV excavations (see Figures 2a and 13b,d,e, a more severe settlement was measured in reality for the SE-NE corner (SB14). The reason of reading higher settlement from SB14 monitoring bolt might be due to a possible local discontinuity and stiffness difference in the relatively thick and loose man-made fill. The region has been a trade and residential center over the centuries and many archaeological relics including ancient building parts and wells have been discovered (Figure 14) (Iwano et al. 2013).
(2) Since the influence of other neighboring tunnels (SPF, CE, and ISL) cannot be considered in the generation of the combined settlement field, the magnitudes of the estimated combined settlements is slightly lower than the measured values. Although these excavations contributed to an extent to the settlement of the mosque, they cannot be included in the settlement field calculations due to geometrical difficulties. In order to consider the effect of SPF and CE, interaction between SPF&CE and shaft wall should be investigated by further analyses. Similarly, accounting for the effect of ISL excavation that have a different alignment (sloping upward to the ground surface) would require physical modeling of this excavation in 3D.

Despite these limitations, the generated settlement fields are believed to reflect the basics of the ground movements near the Hoca Pasha Mosque.

5.2.3 Second-stage analysis results

The second-stage analyses are performed using the combined 3D settlement field shown in Figure 13f and (Table 7). The Analyses 1 (reference), 2, and 3 aim to investigate the effect of the Young's modulus of the masonry. Analyses 1, 4, 5, and 6 investigate the effect of the bedding stiffness using a constant Young's modulus of the masonry. Analyses 7 and 8 study the effect of the leaving out the pre-existing crack and bedding interfaces, respectively. In analysis 9 both interfaces have been left out.

Note that all these are linear analyses, based on the following assumptions.

(i) The bedding interface will remain under compression when considering all loads: any potential separation between soil and building is surpassed.
(ii) The crack interfaces will remain open: the need for an increased stiffness value in case of a crack closure is left out.

Using constant stiffness properties for these interfaces is then justified. It has been verified that with the inclusion of the building weight all bedding interfaces will indeed remain under compression for all analyses. The crack interfaces represent cracks with an initial

Figure 14. Archaeological building remains in a shaft excavation in the region.

Table 7. The features of the parametric analyses.

Property	Analysis 1 (reference)	Analysis 2	Analysis 3	Analysis 4	Analysis 5	Analysis 6	Analysis 7	Analysis 8	Analysis 9
Young's modulus of the masonry (E_{mi}) (MPa)	350	1000	10000	350	350	350	350	350	350
Bedding stiffness (k_{bz}) (kN/m^3)	40,000	40,000	40,000	5000	20,000	80,000	40,000	No bedding	No bedding
Presence of pre-existing cracks	Yes	Yes	Yes	Yes	Yes	Yes	No	Yes	No
Used settlement field	Combined (Figure 14f)	Combined (Figure 14f)	Combined (Figure 14f)	Combined (Figure 14f)	Combined (Figure 14f)	Combined (Figure 14f)	Combined (Figure 14f)	Combined (Figure 14f)	Combined (Figure 14f)

crack opening in the range of 5–10 mm. No detailed information about the exact openings is available. For some of the cracks and for some analyses a maximum closure is observed of 10 mm for a part of the crack, which thus suggests a full closure of cracks at some locations and would demand for an increase of interface stiffness. However, this effect has been left out in the analyses, since the occurrence of possible crack closures is very limited and because of the limited available data on initial cracks openings. An additional advantage of linear analyses is that superposition allows to analyse only the effect of the settlement loads which will facilitate the interpretation of the results.

The contours of the principal tensile strain (ε_p) and relative displacements of the crack and bedding interfaces (δ_{cz}) obtained through the Analyses 1–9 are presented in Figures 15–17. In addition, the ranges of the variation of the openings and closings throughout the concerned crack and bedding interfaces are shown comparatively in the Appendix in Figure A1 for each analysis. Note that, in Figure A1, while negative values show closings positive values show either openings in the crack interfaces or partial unloading of bedding interface from one compressed state of the soil to another. The values illustrated by the red circles are the in-situ crack measurements at the end of July 2011.

The results of Analyses 1, 2, and 3 show that an increasing structural stiffness through the increase of the Young's modulus of the masonry walls affects the conformity of the walls to the applied prescribed deformations. The more homogenous distribution of the bedding displacements (relative displacements of the bedding interface are being close to zero) in Analysis 1 indicates that the structure, which has the lowest stiffness, mostly conforms to the applied prescribed deformations (Figures 15 and A1). This situation eventually results in higher principal tensile strains within the structure. Increasing structural stiffness results in increased relative displacements in the bedding interface (Figures 15 and A1). The magnitude of the maximum principal tensile strain decreases and the structure tends to remain undeformed. This result is completely in line with the findings of previous studies of Potts and Addenbrooke (1997) and Son and Cording (2005). They established a relationship between soil/structure stiffness ratio and potential building distortions and observed that as this ratio decreases, the building distortions decrease.

As the structural stiffness increases, C1 tends to widen at its bottom part and close at its upper part in a more pronounced manner. The C2 acts the other way around due to rotation of the wall portion between C1 and C2 crack interfaces as observed in the first stage analysis of NE wall in Section 5.1. The summed magnitude of the relative displacements of C5 and C6 crack interfaces decreases slightly. Cracks C3-1 and C3-2 have the lowest relative displacement regardless increasing stiffness. As the Young's modulus increases, C10 changes to a partial opening from a closure (Figures 15 and A1).

Increase of the soil stiffness is simulated with the increase of bedding stiffness. As the bedding stiffness is increased from k_{bz1} to k_{bz4} (through the Analyses 4, 5, 1, and 6, respectively) a remarkable increase of principal tensile strain in the walls is observed (Figures 15 and 16). This is because higher bedding stiffness yields higher stress in comparison to a soft bedding subjected to same magnitude of prescribed settlement deformation. Recall that increasing soil/structure stiffness ratio results in increases of the structural distortions. On the other hand, a stiffer bedding interface leads to a more uniform relative displacement distribution which almost equals to zero in magnitude (see Analysis 6). As the bedding stiffness increases, the relative displacements of the localized cracks change insignificantly. Analysis 8 can be considered as the extreme case in terms of the bedding stiffness ($k_{bz} \rightarrow \infty$). For this analysis, while an increase in the tensile principal strain values is observed, the relative displacements of the localized cracks are similar to those obtained for other bedding stiffness values.

Finally, comparing the results of Analyses 1 & 7 and 8 & 9 shows that the presence of pre-existing cracks reduces the principal tensile strains in the close vicinity of the cracks, but results in an increase in other neighboring sections

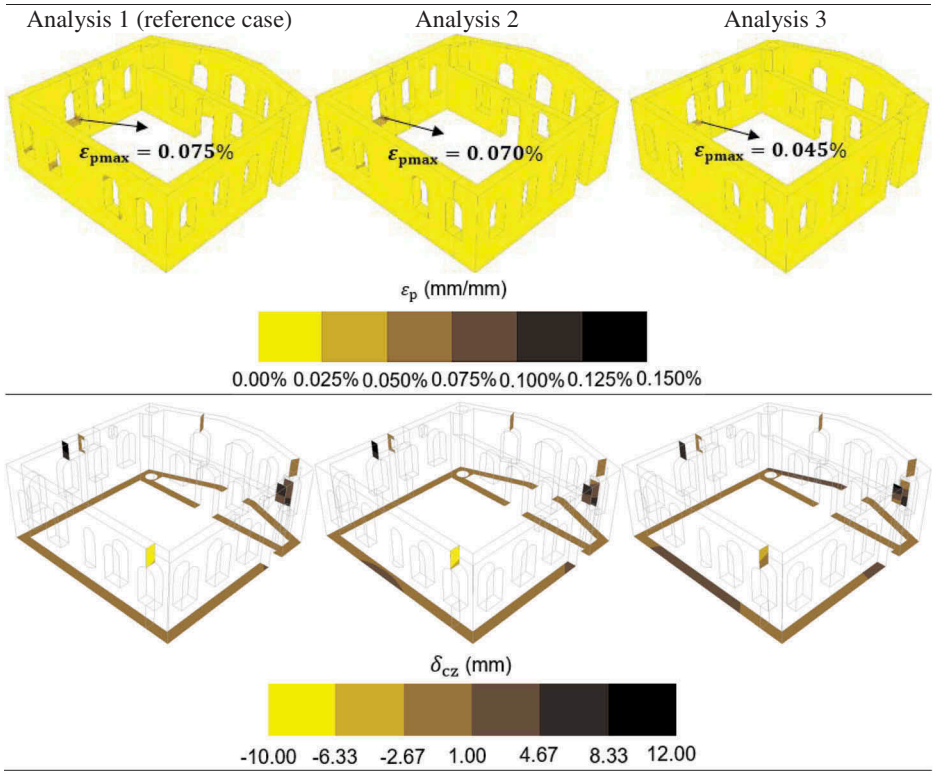

Figure 15. The results of the Analyses 1, 2, and 3 (variation of the masonry stiffness).

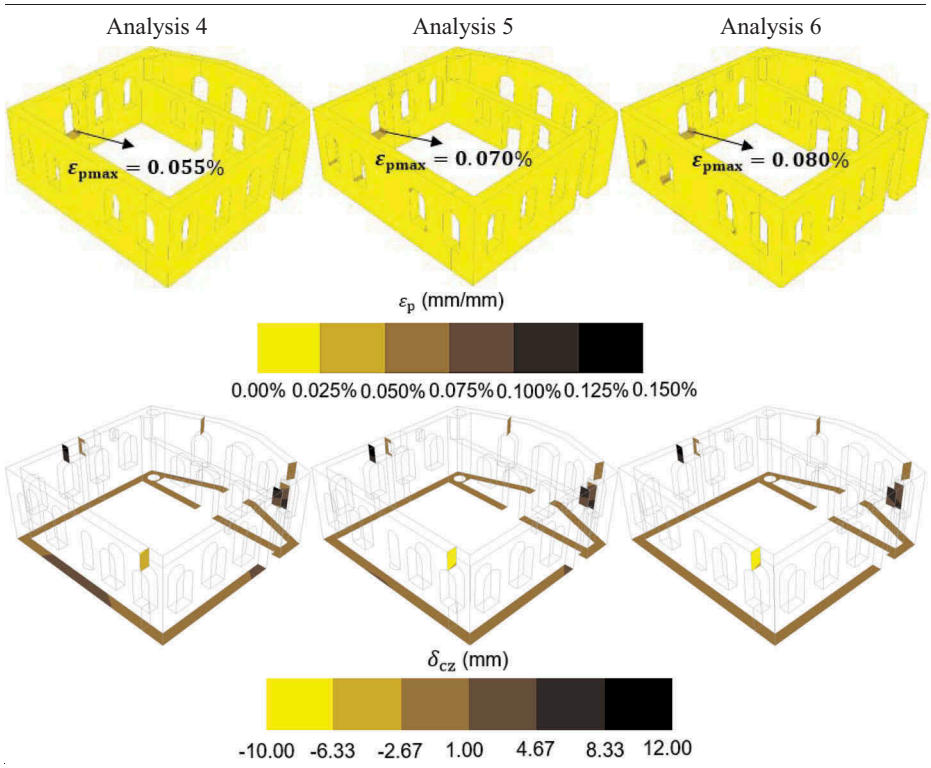

Figure 16. The results of the Analyses 4, 5 and 6 (variation of the bedding stiffness).

(Figure 17). This result was also observed in the previous Section 5.1 in which each wall was examined separately. Since the model used in Analysis 9 does not include crack interfaces, a concentration of principal tensile strain appears at the upper sections of the SW and NE walls. Although principal tensile strains reach the highest

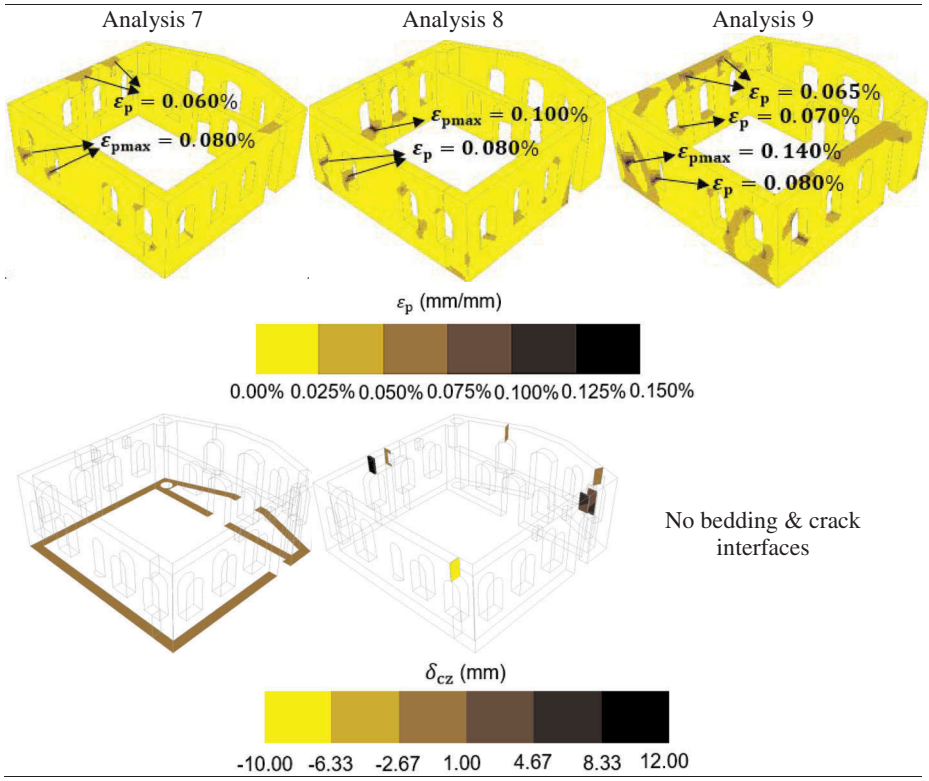

Figure 17. The results of the Analyses 7, 8, and 9 (variations of pre-existing cracks and bedding).

magnitude in Analysis 8 and 9, the maximum principal tensile strain does usually not exceed 0.14% which corresponds to slight damage according to Table A1. This result is also in line with the results found in previous section and site observations.

6. Conclusions

The settlement response of the historic Hoca Pasha Mosque to a nearby network of shaft and tunnel excavations is numerically examined. The problem has a series of challenges due to uncertainties regarding mostly the excavation activities, soil properties, building material and pre-existing damages. These typical difficulties are inherently encountered in such case studies. In order to put off some of these uncertainties a two-stage analysis approach is adopted. First the 3D structural model (with and without existing cracks) is verified in a way that each façade wall is loaded separately using the measured settlements and taking into account flange affects (stiffness contribution) of other connecting walls. This stage to a large extend reduces modeling uncertainties. In the second stage, the effects of other parameters, i.e., the building stiffness, bedding stiffness and combined settlement field due to sequential excavation works are investigated. This naturally increases the modeling uncertainties, but is closer to the practice of *predicting* settlement responses.

The following conclusions can be derived from the reproduced response of the mosque.

(i) Using a two-stage analysis approach, the actual response of the building can be satisfactorily represented. Despite the serious simplifications in modeling, the overall settlements and crack activities could be simulated realistically. In accordance with the site observations, analysis results showed that the tensile strains in the walls are usually of relatively limited magnitude: a few new cracks of insignificant extent occurred due to settlements.
(ii) Including existing cracks into modeling through the discrete interfaces reduces tensile strains in the close vicinity but results in an increase in the tensile strains of other neighboring. While the activity of the existing cracks is considerably influenced by the increase of the Young's modulus of masonry, the variation of the bedding stiffness in the considered range has a limited effect.
(iii) Excluding both bedding and existing crack interfaces during modeling results in the most severe case in terms of tensile strain level and tensile strain distribution.

Besides the examination of the specific case of historic Hoca Pasha Mosque, the performed parametric analyses

supported by the sub-studies regarding the determination of 3D settlement fields also provide useful outputs to reach more generalizable results. The obtained results confirm the previous findings in the literature.

(i) Increased structural stiffness through the increase of the Young's modulus of the masonry walls reduces the conformity of the structure to the applied prescribed settlements and leads to lower tensile strains.
(ii) Increase of the soil stiffness is simulated with the increase of the bedding stiffness. The higher the bedding stiffness is the more the structure conforms to the applied prescribed settlements. This eventually results in increased tensile strains. As an extreme condition, excluding bedding interface corresponds to a case with infinite bedding stiffness.

Acknowledgments

The authors would like to express their thanks to DLH Marmaray Directorate General for their permission to use the project information. Special thanks are due Mr. Gokbora Akay, control manager of the project, who generously gave of his time to help with the project details. The architectural suggestions of Ms. Nurcan Sefer and in-situ drawings of Mr. Dogan Akgun is appreciated. The authors also thank to Mr. Maziar Partovi and Mrs. Hee-Jeong Kang from DIANA FEA BV for the technical support.

Funding

This work was financially supported by the Scientific and Technological Research Council of Turkey (TUBITAK) [2214-A scholarship reference number: 1059B141500705].

References

Akgun, D. 2016. Marmaray çalışması hk. *Message to the first author*, April 28. Email.
Amorosi, A., D. Boldini, G. De Felice, M. Malena, and M. Sebastianelli. 2014. Tunnelling-induced deformation and damage on historical masonry structures. *Géotechnique* 64:118–30. doi:10.1680/geot.13.p.032.
Boscardin, M. 1980. Building response to excavation-induced ground movements. Ph.D. Thesis, University of Illinois at Urbana-Champaign, Champaign, IL.
Boscardin, M. D., and E. J. Cording. 1989. Building response to excavation-induced settlement. *Journal of Geotechnical Engineering* 115:1–21. doi:10.1061/(asce)0733-9410(1989)115:1(1).
Bowles, J. E. 1996. *Foundation analysis and design*. McGraw-Hill Companies, Inc., New York, USA.
Bryson, L. S., and M. J. Kotheimer. 2011. Cracking in walls of a building adjacent to a deep excavation. *Journal of Performance of Constructed Facilities* 25:491–503. doi:10.1061/(asce)cf.1943-5509.0000185.
Burd, H. J., G. T. Houlsby, C. E. Augarde, and G. Liu. 2000. Modelling tunnelling-induced settlement of masonry buildings. *Proceedings of the Institution of Civil Engineers - Geotechnical Engineering* 143:17–29. doi:10.1680/geng.2000.143.1.17.
Burhouse, P. 1969. Composite action between brick panel walls and their supporting beams. *Proceedings of the Institution of Civil Engineers* 43:175–94. doi:10.1680/iicep.1969.7381.
Burland, J., B. Broms, and V. de Mello. 1977. Behavior of foundations and structures. 9th International Conference on Soil Mechanics and Foundation Engineering, Tokyo.
Burland, J., J. Standing, and F. Jardine. 2001. *Building response to tunneling: Case studies from construction of the jubilee line extension, London. CIRIA special publication series*. London: Thomas Telford.
Burland, J., and C. Wroth. 1974. Settlement of buildings and associated damage. Proceedings of conference on settlement of structures, Cambridge.
Caspe, M. S. 1966. Surface settlement adjacent to braced open cuts. *Journal of Soil Mechanics and Foundations Division* 92:51–59.
Clough, G. W., and T. D. O'Rourke. 1990. Construction induced movements of in-situ walls. *Design and Performance of Earth Retaining Structures-Proceedings of a Conference* 25:439–70.
Detail Survey Report Existing Damage Assessment Risk Evaluation for Buildings in Sirkeci Area Package 1 (internal). 2008. Taisei Gama Nurol joint venture. Marmaray Project - Contract BC1, Istanbul.
DIANA v10.1. 2016. DIANA FEA BV, Delft, Netherlands
Fargnoli, V., C. G. Gragnano, D. Boldini, and A. Amorosi. 2015. 3D numerical modelling of soil–Structure interaction during EPB tunnelling. *Géotechnique* 65:23–37. doi:10.1680/geot.14.p.091.
Finno, R. J., S. Bryson, and M. Calvello. 2002. Performance of a stiff support system in soft clay. *Journal of Geotechnical and Geoenvironmental Engineering* 128:660–71. doi:10.1061/(ASCE)1090-0241(2002)128:8(660).
Fu, J., J. Yang, X. Zhang, H. Klapperich, and S. M. Abbas. 2014. Response of the ground and adjacent buildings due to tunnelling in completely weathered granitic soil. *Tunnelling and Underground Space Technology* 43:377–88. doi:10.1016/j.tust.2014.05.022.
Geological Report for Sirkeci Station West Ventilation Shaft (internal). 2008. Taisei Gama Nurol joint venture. Marmaray Project - Contract BC1, Istanbul.
Giardina, G., M. A. N. Hendriks, and J. G. Rots. 2015. Sensitivity study on tunnelling induced damage to a masonry façade. *Engineering Structures* 89:111–29. doi:10.1016/j.engstruct.2015.01.042.
Ispir, M., and A. Ilki. 2013. Behavior of historical unreinforced brick masonry walls under monotonic and cyclic compression. *Arabian Journal for Science and Engineering* 38:1993–2007. doi:10.1007/s13369-013-0567-4.
Istanbul Technical University (ITU) Technical Evaluation Reports for Hoca Pasha Mosque in Sirkeci Area (internal). 2008-2011. Marmaray Project - Contract BC1, Istanbul.
Iwano, M., S. Kobayashi, T. Kaneko, K. Ikeda, Y. Shimizu, and S. Sakurai. 2013. Construction of deep underground

railways station and cross over tunnels in historical area, Istanbul, Turkey. In *World tunnel congress*, eds. G. Anagnostou, and H. Ehrbar, Geneva, Switzerland: Taylor & Francis. ISBN 978-1-138-00094-0.

Korff, M., R. J. Mair, A. F. Van Tol, and F. J. Kaalberg. 2012. The response of piled buildings to deep excavations. In *Geotechnical aspects of underground construction in soft ground*, ed. G. Viggiani, London: Taylor & Francis. ISBN 978-0-415-68367-8.

Lee, S. J., T. W. Song, Y. S. Lee, Y. H. Song, and I. K. Kim. 2007. A case study of building damage risk assessment due to the multi-propped deep excavation in deep soft soil. 4th International Conference of Soft Soil Engineering, Vancouver, London, Taylor Francis.

Long, M. 2001. Database for retaining wall and ground movements due to deep excavations. *Journal of Geotechnical and Geoenvironmental Engineering* 127:203–24. doi:10.1061/(asce)1090-0241(2001)127:3(203).

Losacco, N., A. Burghignoli, and L. Callisto. 2014. Uncoupled evaluation of the structural damage induced by tunnelling. *Géotechnique* 64:646–56. doi:10.1680/geot.13.p.213.

Lourenco, P. 1996. Computational strategies for masonry structures. Ph.D. Thesis, Delft University of Technology, Delft, Netherlands.

Marmaray Project Pressuremeter Test Results in the content of Sirkeci Ebusuud Street Shaft (internal). 2009. Geoteknik. Marmaray Project - Contract BC1, Istanbul.

Method Statements for Excavation and Support Works of Sirkeci Station West Ventilation Shaft and NATM Tunnels (internal). 2008. Taisei Gama Nurol Joint Venture. Marmaray Project - Contract BC1, Istanbul.

Meyerhof, G. G. 1982. Limit states design in geotechnical engineering. *Structural Safety* 1:67–71. doi:10.1016/0167-4730(82)90015-7.

Monthly Geotechnical Monitoring Reports (internal). 2008–2013. Taisei Gama Nurol joint venture. Marmaray Project - Contract BC1, Istanbul.

Moormann, C. 2004. Analysis of wall and ground movements due to deep excavations in soft soil based on a new worldwide database. *Soils and Foundations* 44:87–98. doi:10.3208/sandf.44.87.

Peck, R. 1969. Deep excavations and tunneling in soft ground. Proceedings of the 7th international conference on soil mechanics and foundation engineering, Mexico.

Pickhaver, J. A., H. J. Burd, and G. T. Houlsby. 2010. An equivalent beam method to model masonry buildings in 3D finite element analysis. *Computers & Structures* 88:1049–63. doi:10.1016/j.compstruc.2010.05.006.

Polshin, D., and R. Tokar. 1957. Maximum allowable non-uniform settlement of structures. Proceedings of the fourth international conference on soil mechanics and foundation engineering, London.

Potts, D. M., and T. I. Addenbrooke. 1997. A structure's influence on tunnelling-induced ground movements. *Proceedings of the Institution of Civil Engineers - Geotechnical Engineering* 125:109–25. doi:10.1680/igeng.1997.29233.

Prediction of Ground Surface Settlement Based on Back Analysis for Sirkeci Station (internal). 2011. Taisei Gama Nurol joint venture. Marmaray Project - Contract BC1, Istanbul.

Pujades, E., E. Vázquez-Suñé, L. Culí, J. Carrera, A. Ledesma, and A. Jurado. 2015. Hydrogeological impact assessment by tunnelling at sites of high sensitivity. *Engineering Geology* 193:421–34. doi:10.1016/j.enggeo.2015.05.018.

Rankin, W. 1988. Ground movements resulting from urban tunnelling: Predictions and effects. *Geological Society, London, Engineering Geology Special Publications* 5 (1):79–92. doi:10.1144/GSL.ENG.1988.005.01.06.

Sefer, N., and Z. Ahunbay. 2015. The waqf culturel heritage of Istanbul's Eminonu district- An assessment of the conservation status in the period 1920-2015 (in Turkish). *Restorasyon Yilligi Dergisi* 10:78–120. ISSN:2146-3166.

Son, M. 2003. The response of buildings to excavation-induced ground movements. Ph.D. dissertation, University of Illinois at Urbana-Champaign, Champaign, IL.

Son, M., and E. J. Cording. 2005. Estimation of building damage due to excavation-induced ground movements. *Journal of Geotechnical and Geoenvironmental Engineering* 131:162–77. doi:10.1061/(asce)1090-0241(2005)131:2(162).

Son, M., and E. J. Cording. 2011. Responses of buildings with different structural types to excavation-induced ground settlements. *Journal of Geotechnical and Geoenvironmental Engineering* 137:323–33. doi:10.1061/(asce)gt.1943-5606.0000448.

Appendices

Table A1. Damage classification table (modified from Burland, Broms, and De Mello 1977; Boscardin and Cording 1989).

Category of damage	Damage class	Description of typical damage and ease of repair [a,b]	Approximate crack width[c] (mm)	Limiting tensile strain boundaries (%) after Boscardin and Cording (1989)	
				$\varepsilon_{lim(low)}$	$\varepsilon_{lim(up)}$
Aesthetic damage	0-Negligible	Hairline cracks	Up to 0.1 mm	0.000	0.050
	I-Very slight	Fine cracks that can easily be treated during normal decoration.	Up to 1 mm	0.050	0.075
	II-Slight	Cracks can be easily filled. Cracks are visible externally.	Up to 5 mm	0.075	0.150
Functional damage affecting serviceability	III-Moderate	The cracks require some opening up and can be patched by a mason.	5–15 mm or a number of cracks larger than 3 mm	0.150	0.300
	IV-Severe	Includes large cracks. Extensive repair work is required.	15–25 mm but also depends on the number of cracks	0.300	
Structural damage affecting stability	V-Very severe	Beams lose bearing, walls lean and require shoring, and there is a danger of structural instability.	Usually larger than 25 mm but also depends on the number of cracks	0.300	

[a] Location of damage in the building or structure must be considered when classifying the degree of damage.
[b] Descriptions are shortened for brevity. Refer to Burland, Broms, and De Mello (1977) for full descriptions.
[c] Crack width is only one aspect of damage and should not be used alone as a direct measure of it.

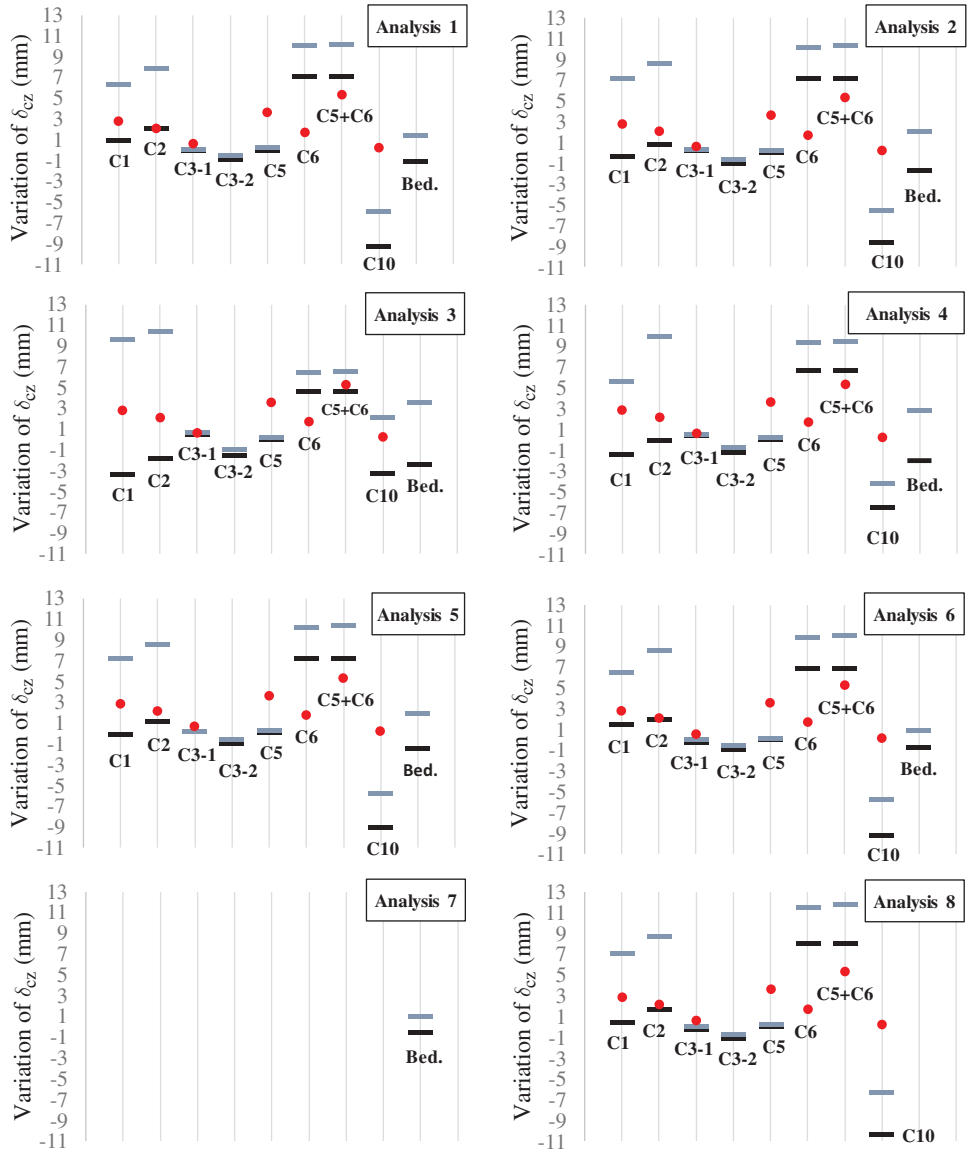

Figure A1. The ranges of variation of relative displacements of crack and bedding interfaces.